

Supplementary Information

Controlled Sculpture of Black Phosphorus Nanoribbons

Paul Masih Das^{1#}, Gopinath Danda^{1,2#}, Andrew Cupo^{3#}, William M. Parkin¹, Liangbo Liang⁴, Neerav Kharche³, Xi Ling⁵, Shengxi Huang⁵, Mildred S. Dresselhaus⁵, Vincent Meunier^{3*}, and Marija Drndić^{1*}

¹Department of Physics and Astronomy, University of Pennsylvania, Philadelphia, Pennsylvania, 19104, USA

²Department of Electrical and Systems Engineering, University of Pennsylvania, Philadelphia, Pennsylvania, 19104, USA

³Department of Physics, Applied Physics, and Astronomy, Rensselaer Polytechnic Institute, Troy, New York, 12180, USA

⁴Center for Nanophase Materials Science, Oak Ridge National Laboratory, Oak Ridge, Tennessee 37831, USA

⁵Department of Electrical Engineering and Computer Science, Massachusetts Institute of Technology, Cambridge, Massachusetts, 02139, USA

[#]These authors contributed equally to this work.

*To whom correspondence should be addressed: meuniv@rpi.edu and
drndic@physics.upenn.edu.

Table of Contents:

- 1. Thickness analysis of few-layer BP flakes on holey carbon grids.**
- 2. BP STEM image simulations.**
- 3. 80 kV HAADF STEM few-layer BP lattice image.**
- 4. Time evolution of suspended few-layer BP nanostructures under electron irradiation.**
- 5. Initial and final geometries for removing single atoms from phosphorene edges.**
- 6. BPNR width and instrument resolution measurements.**
- 7. Band structures for 2D and bulk ZZ-2 edge nanoribbons.**
- 8. Band structures for phosphorene along armchair and zigzag directions.**
- 9. Determination of edge bands around the Fermi level by evaluation of charge density for specific bands.**
- 10. Width dependence of thermodynamic stability for 2D and bulk armchair, ZZ-1, and ZZ-2 edge nanoribbons from the band structure calculations.**
- 11. Thinning of zigzag and armchair BPNRs.**

Section S1: Thickness analysis of few-layer BP flakes on holey carbon grids.

To estimate the thickness of few-layer BP flakes suspended on holey carbon TEM grids, the simplified electron cross-section formula for HAADF STEM imaging was used:

$$\frac{I_p - I_b}{I_c - I_b} = \left(\frac{Z_p}{Z_c} \right)^2 \frac{\rho_p t_p}{\rho_c t_c}$$

Where I_p , I_c , and I_b are the mean image intensities of the few-layer BP flake, carbon film, and background, respectively, as shown in Figure S1. ρ_p (2.69 g/cm^3)¹ and ρ_c (2.15 g/cm^3)² are the densities of black phosphorus and amorphous carbon, respectively, while $Z_p = 15$ and $Z_c = 6$ are the corresponding atomic numbers. t_c is the thickness (20 nm) of the carbon support film and t_p is the unknown thickness of the flake, respectively. The resulting thickness of 17 nm is in good agreement with the sub-20 nm flake thicknesses obtained on holey SiN_x membranes *via* AFM.

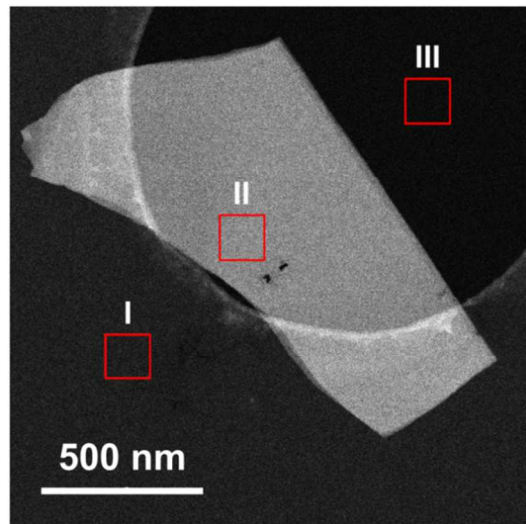


Figure S1. Low-magnification HAADF STEM image of the 17-nm-thick BP flake used to fabricate the nanostructures in Figure 3. Electron image intensities of the carbon film at I, few-layer BP flake at II, and background at III were used to ascertain the flake thickness using the simplified electron cross-section formula.

Section S2: BP STEM image simulations.

STEM images were simulated using the QSTEM package.³ The relaxed geometries of phosphorene and bulk BP obtained from the DFT calculations were used to construct the atomic models. Potential slices were chosen so that single planes of atoms were included in each: two slices for phosphorene and four slices for the unit cell of bulk BP. An array of 200×200 pixels was used and the scattering angle (determined by the probe array size) was set greater than the largest detector angle. The aberration-corrected STEM device parameters used in the simulation are:

Acceleration Voltage: 200 kV

Defocus: 1.729 nm

Astigmatism: 1.613 nm, -60.5 degrees

Spherical Aberration C3: -580 nm

Chromatic Aberration: 1.1 mm

Aberration Spread: 0.4 eV

Convergence Angle: 25 mrad

Detector Inner Angle: 50 mrad

Detector Outer Angle: 180 mrad

The resulting STEM images for phosphorene and AB stacked bilayer BP (single unit cell of bulk BP) are shown in Figures S2.1a and S2.1b, respectively. The observation of a “half lattice constant” scheme indicates the samples are at least bilayer. In Figure S2.2 we justify neglecting thermal diffuse scattering (TDS) in the calculations.

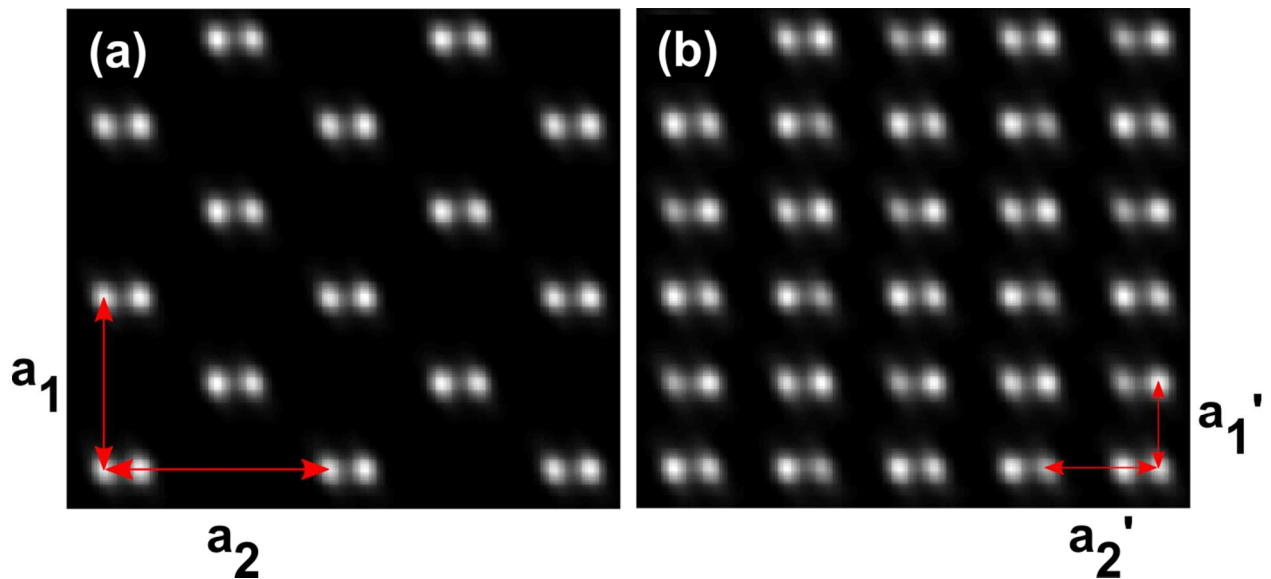


Figure S2.1. STEM simulations of (a) phosphorene indicating full lattice constants (a_1, a_2) and (b) AB stacked bilayer BP from single bulk BP unit cell indicating half lattice constants (a_1', a_2'). The zigzag direction is along a_1 and a_1' and the armchair direction is along a_2 and a_2' .

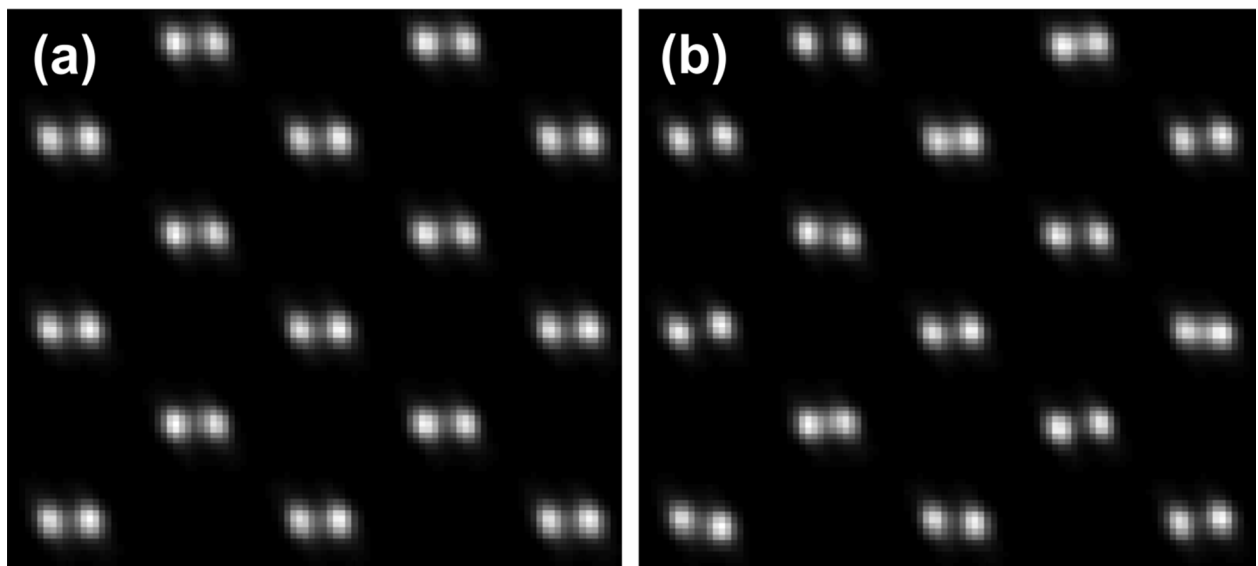


Figure S2.2. To determine the effect of thermal diffuse scattering (TDS), STEM simulations of phosphorene (a) neglecting TDS and (b) including TDS at 293 K were generated. Both images

include 100×100 pixels. The overall difference is negligible for determining structure and therefore we neglected TDS in generating the images in Figure S2.1.

Section S3: 80 kV HAADF STEM few-layer BP lattice image.

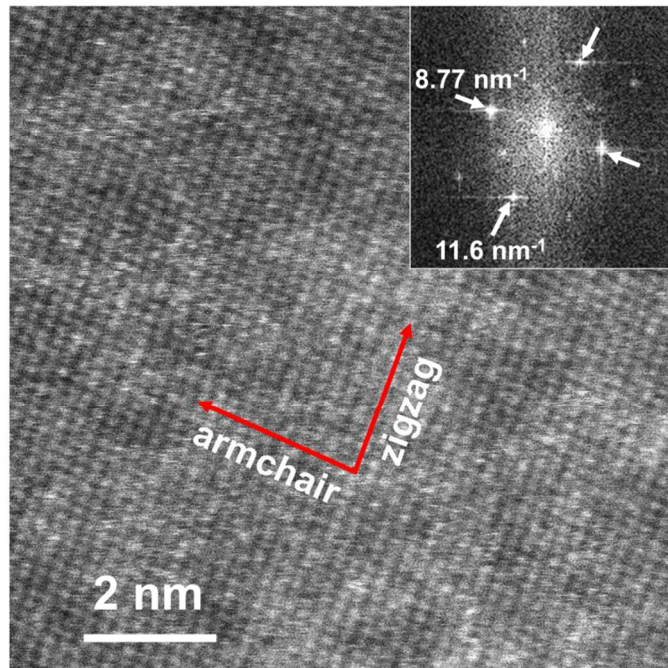


Figure S3. 80 kV HAADF STEM few-layer BP lattice image and (inset) resulting FFT. As expected for the AB-stacked few-layer BP structure (Figure 1c), the reciprocal lattice spacings of 11.6 and 8.77 nm^{-1} closely correspond to a_1' (1.67 \AA) and a_2' (2.24 \AA), the real-space zigzag and armchair half-lattice-constants, respectively. This is in agreement with the results seen at 200 kV (Fig. 1d). The region of interest was tilted to the [001] zone axis prior to imaging.

Section S4: Time evolution of suspended few-layer BP nanostructures under electron irradiation.

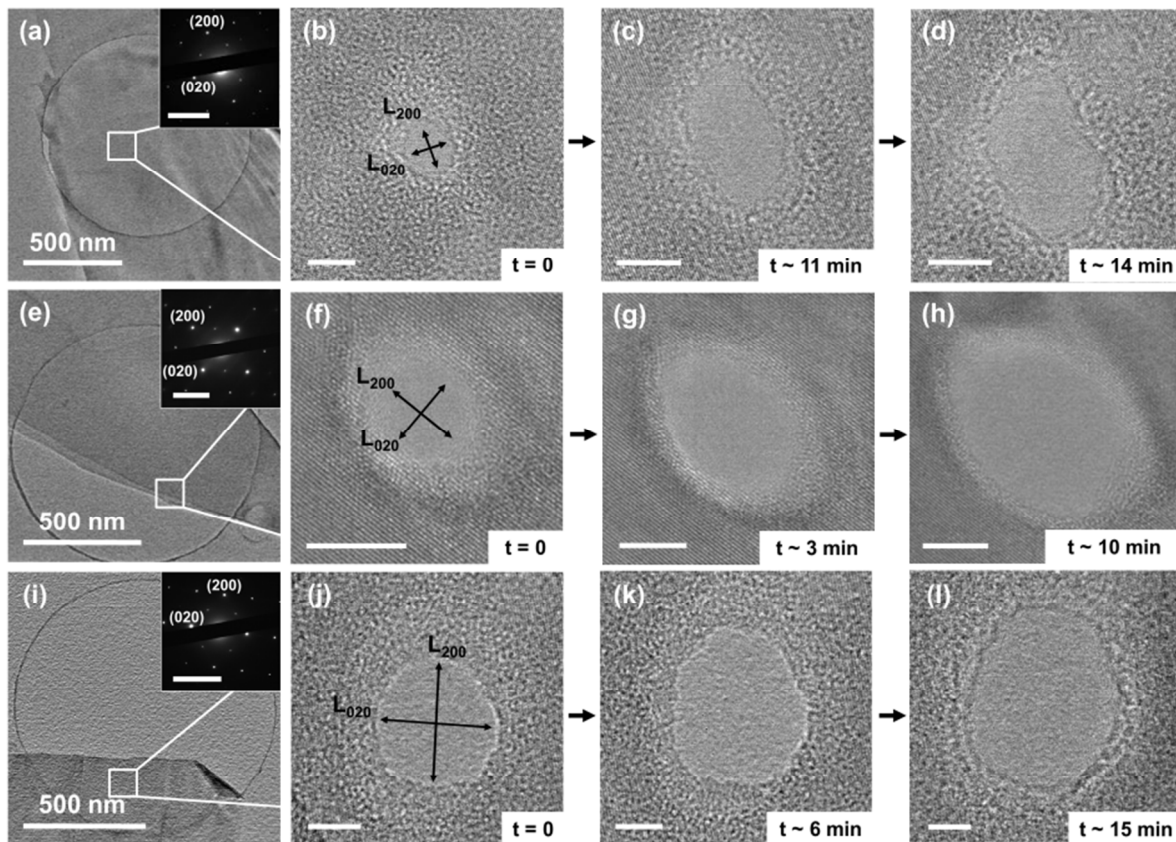


Figure S4.1. Elliptical expansion of suspended BP nanopores under HRTEM constant electron beam irradiation (accelerating voltage = 200 kV, current density = 6.1×10^{-2} pA/nm²) over a period of 10-15 minutes. (a,e,i) The suspended few-layer BP flakes where nanopores were drilled (white squares) and (inset) corresponding diffraction patterns. The ratio between nanopore dimension along zigzag and armchair directions, *i.e.* $L_{200}:L_{020}$, evolved from (b,f,j) 1.0 to (c) 1.9 and (d) 2.0 for row 1, (g) 1.4 and (h) 1.5 for row 2, and (k) 1.2 and (l) 1.4 for row 3. All scale bars in (a) to (l) are 5 nm.

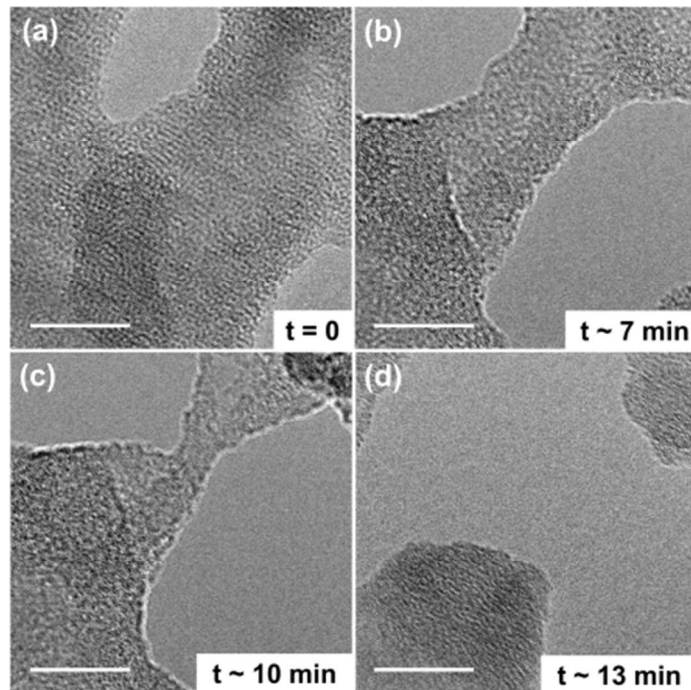


Figure S4.2. Formation of a suspended few-layer BP nanoconstriction under electron irradiation over a period of 13 minutes. (a) HRTEM images of two nanopores separated by a distance of ~ 20 nm. Constant irradiation (current density = 6.1×10^{-2} pA/nm 2) narrows the area between the pores to form nanoconstrictions of narrowest width (b) 10 nm and (c) 3.8 nm until (d) the structure ultimately breaks off and yields a 15 nm gap. All scale bars in (a) to (d) are 10 nm.

Section S5: Initial and final geometries for removing single atoms from phosphorene edges.

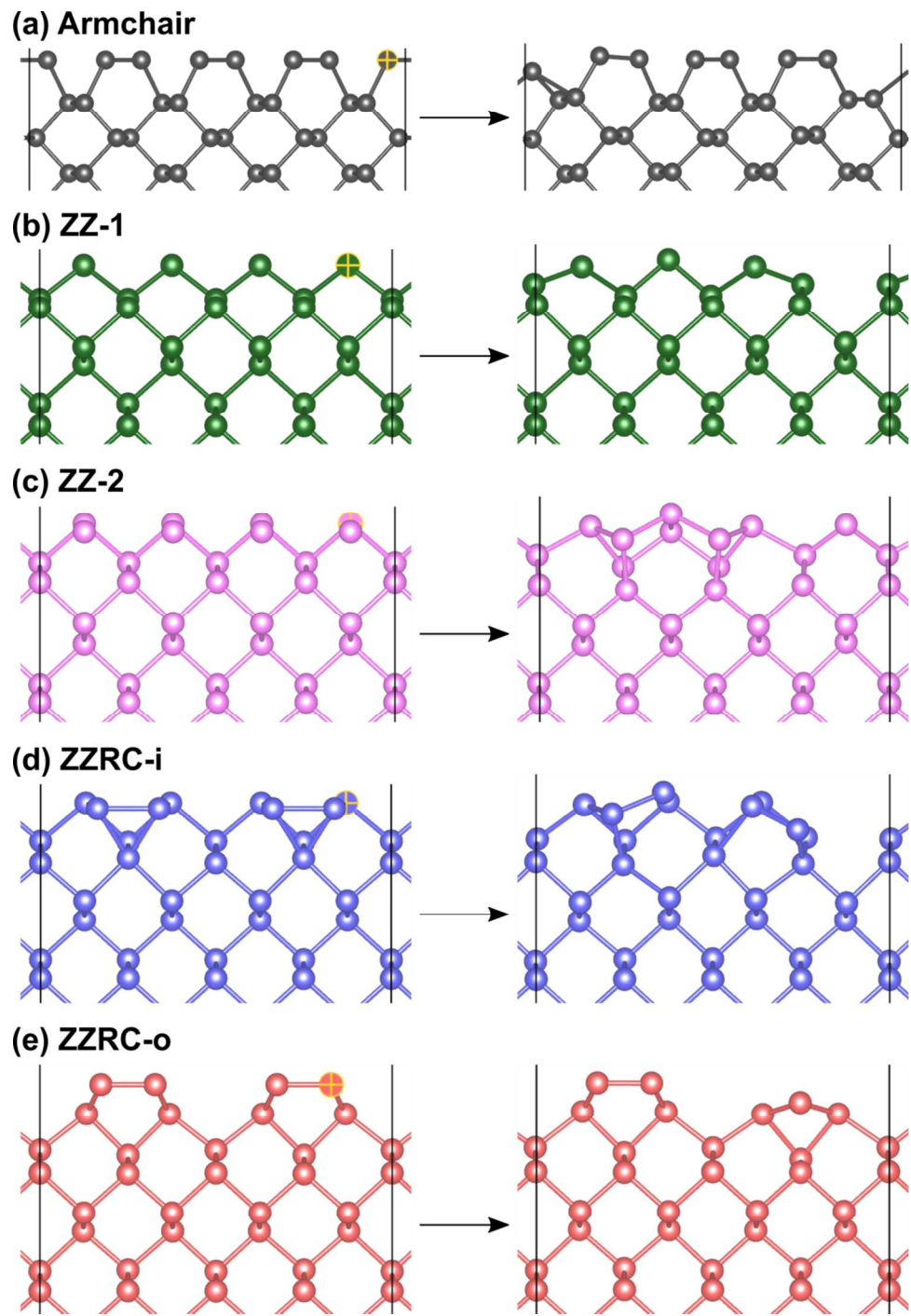


Figure S5. Edge geometries of 4x1 supercells before and after removing single atoms (removed atom indicated by yellow crosshair)⁴ for the (a) AC, (b) ZZ-1, (c) ZZ-2, (d) ZZRC-i, and (e) ZZRC-o edges.

Section S6: BPNR width and instrument resolution measurements.

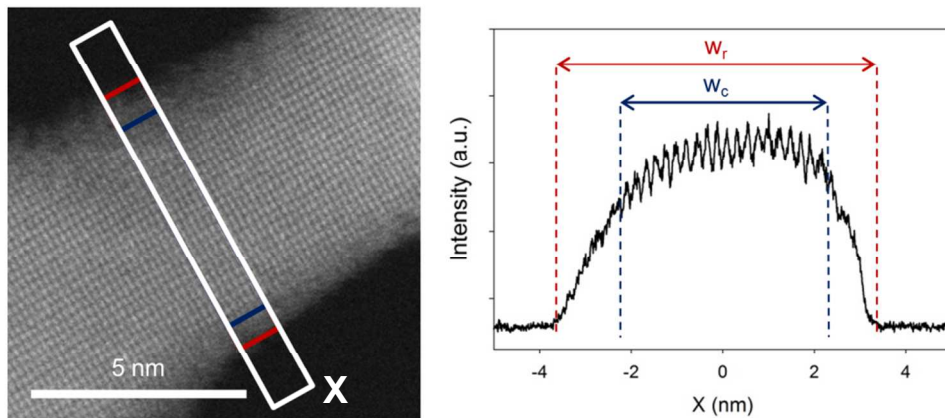


Figure S6.1. Intensity cross-section of the w_r (w_c) = 6.0 (4.6) nm zigzag BPNR from Figure 3b.

Cross-sections were used to measure w_r (total BPNR width) and w_c (crystalline region width). The region w_c is characterized by clear periodic fluctuations in intensity, which are indicative of a periodic atomic structure. The amorphous edge region $w_r - w_c$ also has non-zero intensity, but no periodic structure. The presence of these edges is discussed in the main text.

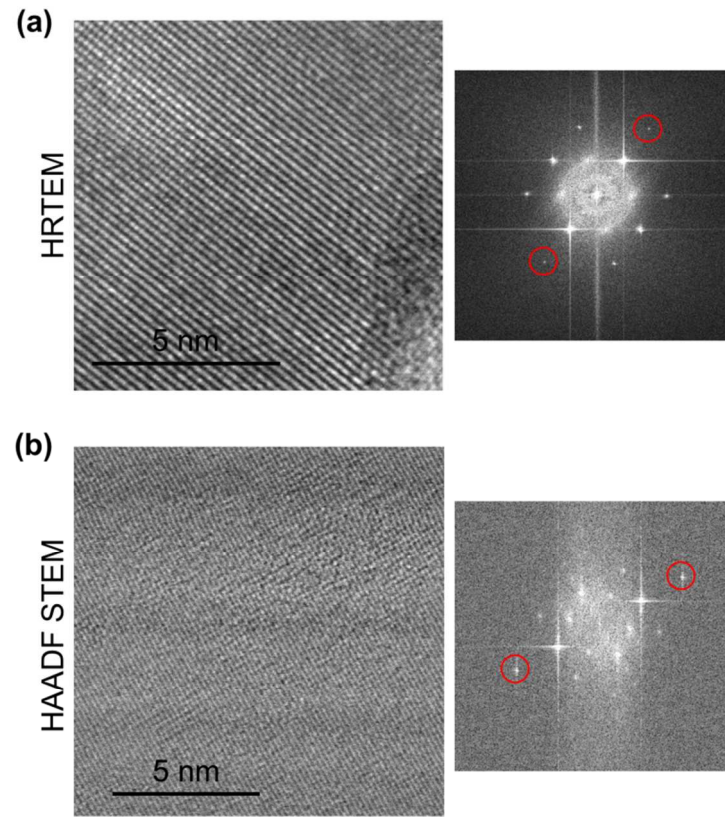


Figure S6.2. Resolution limits for (a) TEM and (b) STEM imaging conditions were obtained by analyzing FFTs of the few-layer BP lattice. The resolution limit is obtained by analyzing the farthest discernible bright spots (red circles), the so-called transformation limit, in the resulting FFTs.⁵ For HRTEM (JEOL 2010F microscope) and HAADF STEM (JEOL ARM 200CF microscope), we report resolution limits of 0.11 and 0.08 nm, respectively.

Section S7: Band structures for 2D and bulk ZZ-2 edge nanoribbons.

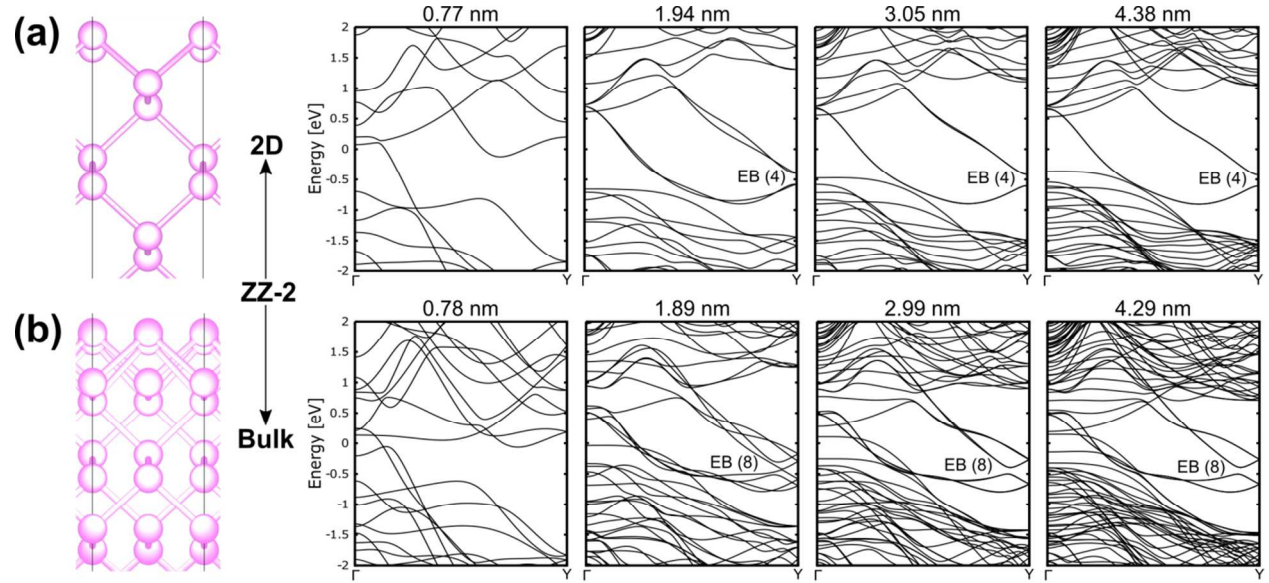


Figure S7. Band structures with the Fermi level set to 0 eV for ZZ-2 edge BPNRs based on the experimentally realized crystalline widths. The edge bands are indicated by EB with the number of such bands in parenthesis for (a) single layer and (b) bulk. All edge bands cross the Fermi level and therefore all nanoribbons are metallic.

Section S8: Band structures for phosphorene along armchair and zigzag directions.

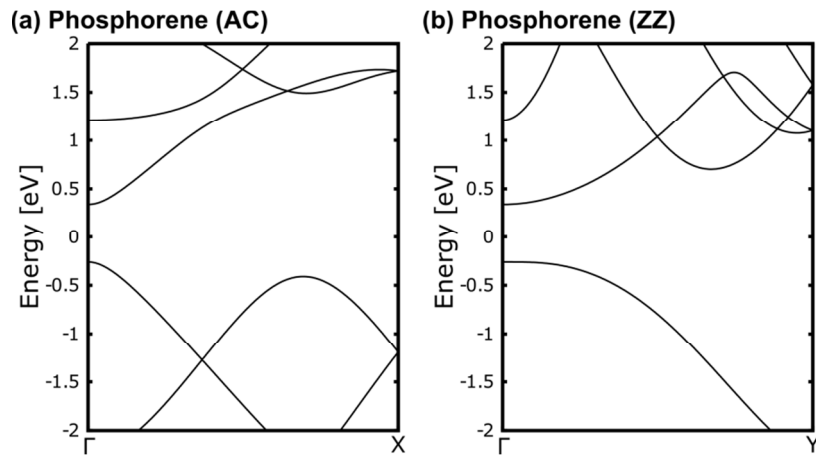


Figure S8. Band structures for phosphorene along (a) armchair and (b) zigzag directions. The edge bands identified in the nanoribbon band structures are absent.

Section S9: Determination of edge bands around the Fermi level by evaluation of charge density for specific bands.

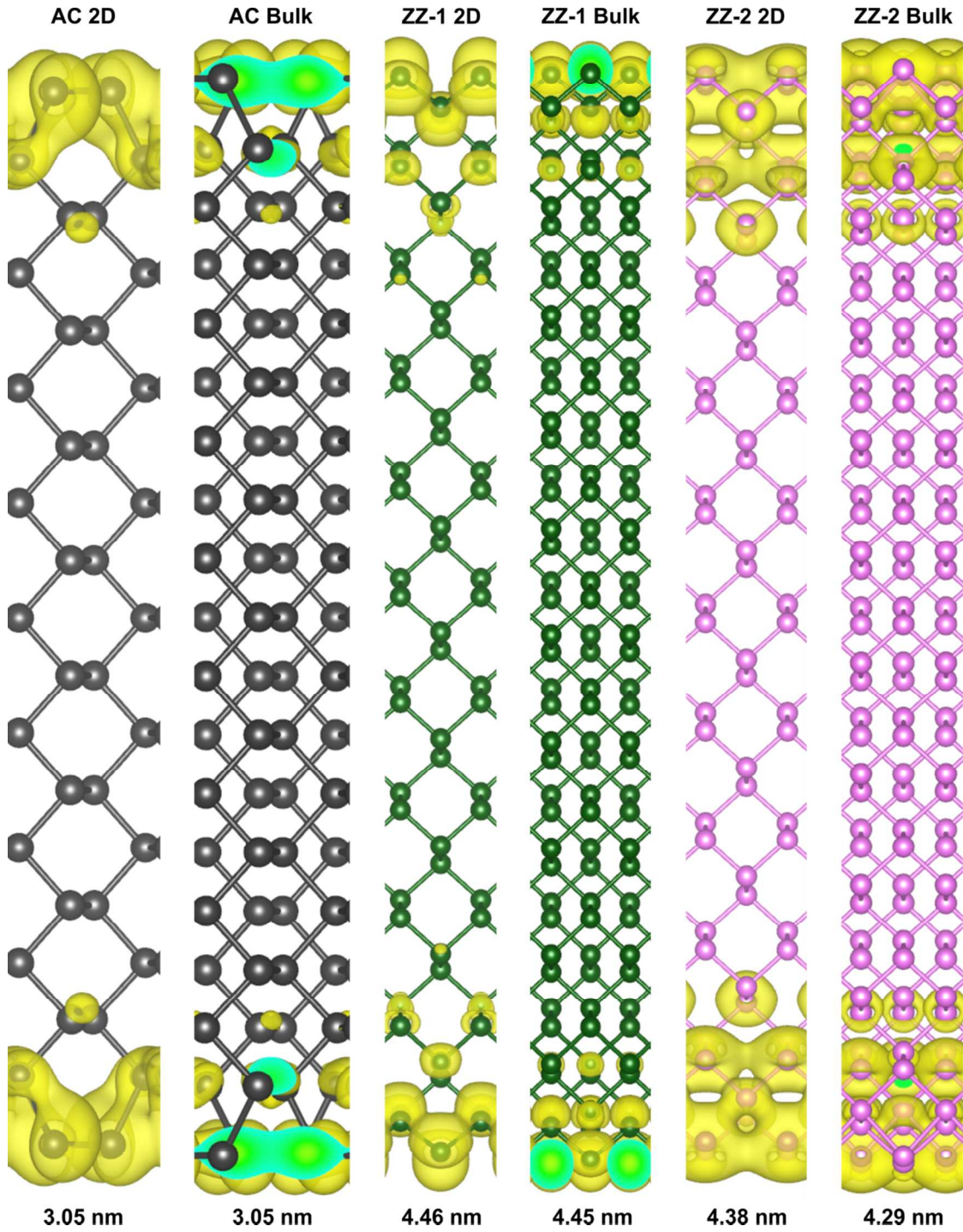


Figure S9. Band-specific charge densities for the edge bands corresponding to the largest width nanoribbons shown in Figure 4 for armchair and ZZ-1, and Figure S7 for ZZ-2.

Section S10: Width dependence of thermodynamic stability for 2D and bulk armchair, ZZ-1, and ZZ-2 edge nanoribbons from the band structure calculations.

For a 2D system, the thermodynamic stability is quantified by the edge energy, which is calculated as $(F_0 - NF_P)/2L$ where F_0 is the total free energy of the system, N is the number of phosphorus atoms, F_P is the free energy per atom for phosphorene, and L is the lattice constant in the direction along the edge. Similarly for the bulk system we calculate the surface energy as $(F_0 - NF_{BP})/2A$ where F_{BP} is the free energy per atom for bulk BP, A is the unit cell area on the surface, and the other symbols are defined similarly. The thermodynamic stability of 2D and bulk armchair, ZZ-1, and ZZ-2 nanoribbons as a function of width is given in Figure S10.

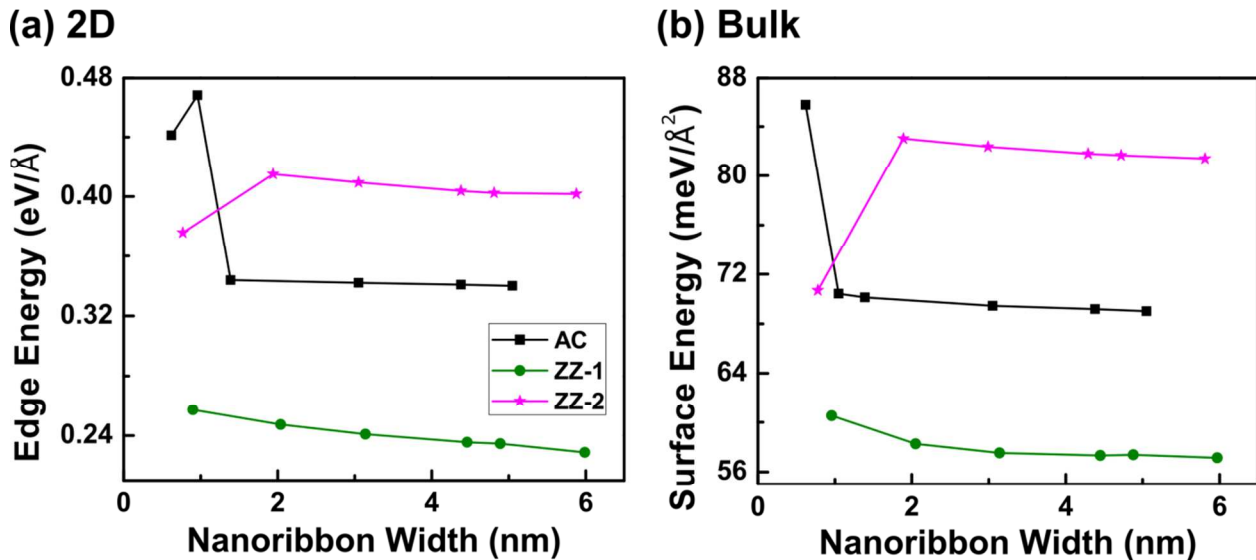


Figure S10. For infinitely long armchair, ZZ-1, and ZZ-2 nanoribbons based on the experimentally realized crystalline widths w_c (Figures 3 and S6.1), the thermodynamic stability was quantified by (a) the edge energy for single layer and (b) the surface energy for bulk. The convergence of the energies with width suggests that long few-nanometer ribbons are stable.

Section S11: Thinning of zigzag and armchair BPNRs.

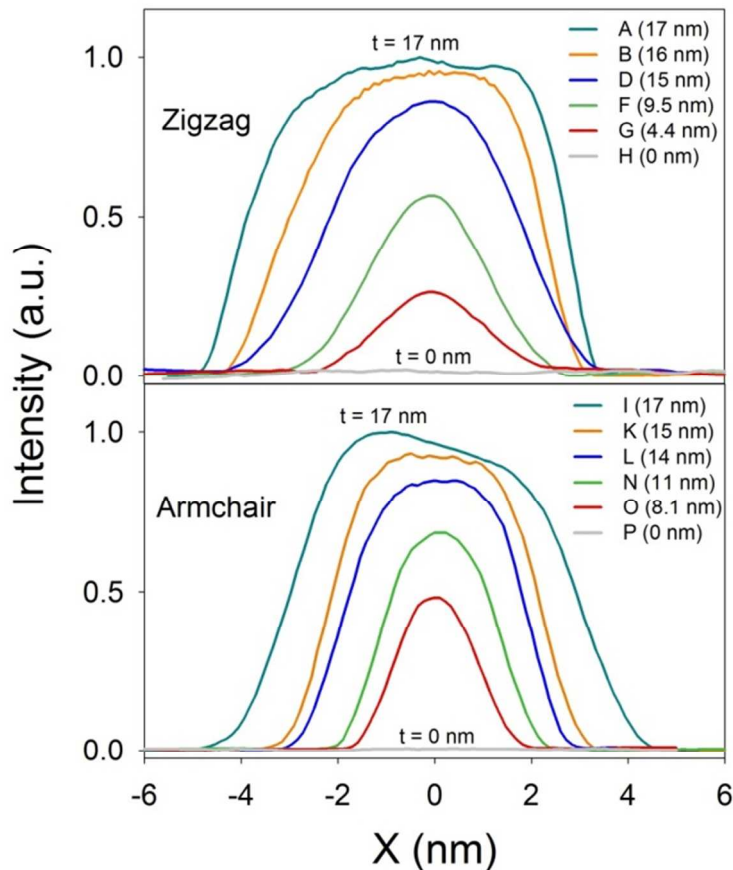


Figure S11. Intensity cross-sections X (Figures 3a,i) of the zigzag (top) and armchair (bottom) BPNRs shown in Figures 3a-h and 3i-p, respectively. Each curve corresponds to a panel in Figure 3 and BPNR thickness determined through the linear HAADF intensity-thickness correlation discussed in the main text. From an initial flake thickness of 17 nm (Figure S1), the zigzag and armchair BPNRs were thinned to minimum thicknesses of 4.4 and 8.1 nm, respectively, before breaking into nanogaps.

References:

- (1) *Semiconductor Materials*; Berger, L.; CRC Press: Florida, 1996; pp 84.
- (2) Iwaki, M. Estimation of the Atomic Density of Amorphous Carbon Using Ion Implantation, SIMS and RBS. *Surf. Coatings Technol.* **2002**, *158*, 377–381.
- (3) *Determination of Core Structure Periodicity and Point Defect Density Along Dislocations*; Koch, C.; PhD Dissertation: Arizona State University, 2002; pp 1-192.
- (4) Momma, K.; Izumi, F. VESTA 3 for Three-Dimensional Visualization of Crystal, Volumetric and Morphology Data. *J. Appl. Crystallogr.* **2011**, *44*, 1272–1276.
- (5) Peng, Y.; Borisevich, A. Y.; Lupini, A. R.; Pennycook, S. J. Resolution Limit Measured by Fourier Transform: 0.61 Angstrom Information Transfer Through HAADF-STEM. *Microsc. Microanal.* **2005**, *11*, 1-2.